

# Contactless Islanding Detection Method Using Electric Field Sensors

Kun-Long Chen<sup>ID</sup>, Member, IEEE, Yi Guo<sup>ID</sup>, Student Member, IEEE,  
 Juncheng Wang<sup>ID</sup>, Graduate Student Member, IEEE,  
 and Xiangguo Yang<sup>ID</sup>, Member, IEEE

**Abstract**—An accurate and cost-effective islanding detection is in a great need for distributed generation (DG) integration. An onsite contactless islanding detection scheme is proposed in this article, based on a small number of tiny and portable electric field (EF) sensors. In contrast to the existing mainstream detection techniques, which are heavily depended on the instrument transformer measurement in substations, the proposed contactless scheme is able to be deployed on the ground below the overhead feeders, enabled by a compact EF sensor and the associated accurate frequency measurement algorithm. The effectiveness, robustness, efficiency, and security advantages of the proposed method are investigated and verified by the simulations using various feeder configurations. It is further supported by the laboratory experiments based on a scale-down overhead feeder testbed.

**Index Terms**—Contactless measurement, distributed generation (DG), islanding detection, overhead line.

## I. INTRODUCTION

AS THE distributed generations (DGs) gain in popularity worldwide, several quintessential safety issues are raised in the electrical industry. Islanding detection has been identified as one of the most significant challenges for integrating distributed generators into the grid. Islanding occurrence leads to several problems on the islanded DG and the connected loads while endangering maintenance personnel. Hence, the antiislanding capability is an essential requirement for DGs connected to power systems, which refers to the capability of a DG to aware of the possible islanding condition, and then to proactively disconnect itself from the islanded system immediately. To the best of our knowledge, most existing islanding detection methods are

Manuscript received August 10, 2020; revised October 25, 2020; accepted November 20, 2020. Date of publication December 8, 2020; date of current version January 6, 2021. This work was supported by the Ministry of Science and Technology, Taiwan (ROC) under Contract MOST 109-2222-E-019-003. The Associate Editor coordinating the review process was Ferdinanda Ponci. (*Corresponding author: Xiangguo Yang*.)

Kun-Long Chen is with the Department of Electrical Engineering, National Taiwan Ocean University, Keelung 202301, Taiwan (e-mail: klchen@mail.ntou.edu.tw).

Yi Guo is with the Department of Mechanical Engineering, The University of Texas at Dallas, Richardson, TX 75080 USA (e-mail: yi.guo2@utdallas.edu).

Juncheng Wang is with the Department of Electrical and Computer Engineering, University of Alberta, Edmonton, AB T6G 2R3, Canada (e-mail: ju4@ualberta.ca).

Xiangguo Yang is with the School of Energy and Power Engineering, Wuhan University of Technology, Wuhan 430070, China (e-mail: yangxiangguo123@163.com).

Digital Object Identifier 10.1109/TIM.2020.3043096

heavily relied on the electrical information (e.g., voltage and current) measured by the instrument transformers, which are installed in substations. Nevertheless, in the most real-world situations, field power engineers always find it is difficult to acquire real-time electrical information from substations due to safety concerns and/or other restrictions. Therefore, future power grids will require an onsite, real-time, contactless (i.e., free of instrument transformers) device, and the associated measurement technique to detect the islanding conditions for continuously integrating DGs.

The remote islanding detection techniques are mainly based on the communication between utilities and DGs. These methods use the supervisory control and data acquisition (SCADA) system [1], [2], the power line carrier communication (PLCC) system [3]–[5], or the wide area measurement system (WAMS) [6], [7] to detect the islanding. These methods monitor the statuses of DGs and utilities to ensure the performance and avoid a nondetection zone (NDZ). However, massive communication apparatuses should be installed in all grid-connected power devices, resulting in the high equipment expense and the follow-up maintenance costs. Additionally, a complicated communication structure also degrades the reliability of the islanding detection system.

Instead of building a communication structure between grid-connected devices, another line of recent research with low cost-efficiency explores the local detection methods, commonly classified into three types: active methods, passive methods, and hybrid methods.

- 1) *Active Methods*: local active techniques are applied by introducing a small disturbance to a power network. The power system will respond to the disturbance with certain patterns indicating its islanding condition. Here lists the several popular active methods and their interesting discussions including Sandia voltage shift (SVS) [8], negative-sequence current injection [9], harmonic current injections [10], active frequency drift (AFD) [11], AFD with positive feedback (AFDPF) [12], [13], Sandia frequency shift (SFS) [14], [15], sliding-mode frequency shift (SMS) [16], [17], fuzzy SFS [18], phase-locked loop (PLL) [19], frequency positive feedback [20], average absolute frequency deviation value (AFDVavg) [21], automatic phase shift (APS) [22], impedance measurement (IM) [23], [24], reactive power variation (RPV) [25], active rate of change of frequency ROCOF) relay [26], harmonic amplification factor [27], and

reactive power perturbation and observation (P and O) in the inverter [28]. Many of these methods have to introduce the disturbance causing undesirable transient. This undesirable transient will lead to power quality issues, definitively reducing the effectiveness of detection and increasing the operational costs.

- 2) *Passive Methods*: local passive techniques detect the islanding situation by directly monitoring system parameters (e.g., voltage magnitude, frequency, phase, and harmonic) at point of common coupling (PCC) on DG's side [29]. An islanding condition is detected when system parameters are changing greatly in a sort of pattern. The most common passive techniques include over/under voltage (OV/UV) [30], over/under frequency (OF/UF) [30], phase jump detection (PJD) [31], ROCOF/rate of change of power (ROCOF/ROCOP) [32], total harmonic distortion (THD) of voltage/current [33], rate of change of phase angle difference (ROCPAD) [34], ROCOF overpower ( $d\bar{f}/dp$ ) [35], oscillation frequency estimation [36], rate of change of voltage and changes in power factors [37], voltage vector shift (VVS) [38], inverter nonlinear effects [39], signature of the pulsewidth modulation (PWM) voltage harmonics [40], negative sequence voltage component [41], and transient component [42]. The aforementioned local passive methods usually come with a large and unavoidable NDZ which may fail the islanding detection. This shortage can be compensated by a combination of the local active and local passive methods, called hybrid methods.
- 3) *Hybrid Methods*: local hybrid methods improve the detection accuracy by combining the advantages of both active and passive techniques. Active methods will be activated to mitigate the large NDZ affects and play a confirmative role only after passive methods detect an islanding situation. The positive feedback combined with the voltage unbalance and THD (VU/THD) was demonstrated in [43]. The article [44] presented the average rate of voltage change combined with the real power shift (RPS). The study [45] proposed SFS combined with ROCOF. The work [46] designed a hybrid islanding detection approach based on the probability of islanding (PoI) at the smart grid (SG) side, and the PoI values were determined using a combination of the passive, active, and the communication islanding detection approaches. The study [47] proposed a nonlinear jumping slip mode frequency shift combined with the reactive power versus frequency. Moreover, the work [48] presented the RPV combined with ROCOF.

Recently, the performance of passive methods has been significantly improved by the rapid development of signal processing and artificial intelligence technologies. Signal processing techniques, such as wavelet transform [49], wavelet packet transform [50], [51], S-transform [52], Hilbert–Huang transform [53], sparse matrix with graph theory [54], and chaos theory [55], help to extract the unique patterns of systems to support a more accurate classification of the islanding/nonislanding situations. However, these methods perform

very well only if the signals are with small noise or noise-free. Additionally, more computation expense and large data storage requirement usually lead to an unsatisfactory detection performance. Artificial intelligent techniques provide a computationally efficient classifier to identify the existence and specific features of various islanding conditions. Different pattern recognition techniques, such as neural network [56], support vector machine (SVM) [57], decision tree (DT) [58], random forest (RF) [59], binary tree (BT) threshold filter [60], adaptive neuro-fuzzy inference system (ANFIS) [61], and adaptive ensemble classifier [62], have been used for the islanding detection.

Overall, the local passive methods are broadly applied for the islanding detection with DGs due to its simple structure and the satisfactory performance. However, none of the existing islanding detection methods (including remote and local methods) works without the electrical information obtained from the substations, which are commonly not available in the practical field measurement applications.

Contactless detection technologies are recently welcome in the field measurement with applications to power systems having DG integration, especially for the scenarios of high-voltage systems, live-line working applications, and so on. Most of the existing technologies for the contactless measurement techniques are mainly built on the electric field (EF) measurement [63]. The study in [64] used eight EF sensors to measure EFs for the geometry evaluation of an overhead line by calculating the three-phase voltage. Zhu *et al.* [65] measured the geometry of the overhead line by magnetic field sensors and calculated the three-phase voltage by three EF sensors. In [66], the actual overhead line geometry was calibrated by the system voltages and the signals from three EF sensors. The overhead line voltages can also be calculated from the measurement signals. Borkowski *et al.* [67] used a single capacitor plate to achieve an accurate busbar voltage measurement inside substations. They used artificial neural network (ANN) to build the circuit model of the stray capacity and the single capacitor plate. In [68], a two-axis capacitance sensor was proposed for evaluating the voltage sequence and the voltage levels of the overhead lines. Issouribehere *et al.* [69] measured the voltage distortion for the overhead lines by a single capacitor plate with a height of 2 m.

A contactless islanding detection method is proposed in this article, which is easy-to-use in the field measurement. A remote measurement technology is designed to capture the voltage frequencies of the measured feeders. Based on such measurement, an islanding detection scheme is proposed as shown in Fig. 1. In the normal condition (without islanding situation), the frequencies of the DG and the main power grid are identical. When an islanding happens, the circuit breaker (CB) will disconnect the DG from the main grid, and their frequencies may not be the same. The frequency difference between the grid and DGs is utilized as the index to identify the islanding condition. Single-axis EF sensors are designed to remotely obtain voltage frequencies of the two overhead feeders connecting DG and power grid. EF sensors are simply placed on the ground out of the substation, and are closed to the locations under the measured feeders.

TABLE I  
COMPARISON OF THE EXISTING METHODS AND THE PROPOSED METHOD

		Technology	Impact on power quality	Cost	NDZ (Power mismatch)	Field measurement <sup>1</sup>
Remote	Communication based methods	Very complicated	No	Very high · Massive sensors · Massive telecommunication devices	None	No
Local	Active methods	Medium	Yes	Medium · Power electronic device used to inject disturbances · Measurement device	None – Small · Negative-sequence current injection [9]: none · Harmonic current injection [10]: none · SFS [15]: depends on its design parameters · AFDVavg [21]: none · APS [22]: depends on its design parameters · RPV [25]: none · Active ROCOF [26]: none · reactive power P&O [28]: none	No
	Passive methods	Simple	No	Low · Measurement device	None – Large · ROCOF [32]: <15% · ROCPAD [34]: none · $df/dp$ [35]: <20% · Oscillation frequency [36]: <1.6% · Voltage vector shift [38]: <5% · Negative sequence voltage component [41]: none · Transient Component [42]: none	No
	Hybrid methods	Complicated	Yes	High · Combination of active and passive methods	None – Small · Average rate of voltage change combined with RPS: none · SFS combined with ROCOF [45]: smaller than SFS · PoI [46]: none · RPV combined with ROCOF [48]: none	No
	Proposed method	Simple	No	Low · Measurement device as shown in Fig. 6	None – Large · The proposed method belongs to the passive methods	Yes

<sup>1</sup> Outdoor field measurement without electrical information from substations.

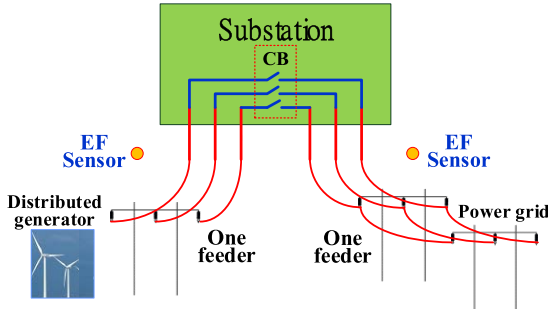


Fig. 1. Proposed EF-sensor-based islanding detection technique.

The proposed method is classified into the local passive detection techniques. But it measures the electrical parameters at both DG and grid sides simultaneously, instead of utilizing only DG information in traditional passive approaches.

Table I summarizes a comparison between the existing methods and the proposed method. All listed local methods tradeoff the performance between the cost, the technology level, and the NDZ [29], [70]. However, only the proposed method can achieve the islanding detection without 1) electrical information from substations and 2) complicated communication structure, through the actual field measurement. With the designed EF sensor and proposed frequency calculation algorithm, the proposed contactless islanding detection method can directly catch the voltage frequencies of the measured

feeders, thus the field measurement can be performed. Besides, this simple measurement scheme of the proposed contactless islanding detection method is also with the following characteristics: 1) low price; 2) on-site access-friendly structure; 3) user-friendly; 4) portability; and 5) safety to avoid from the electric shock.

The remainder of this article is organized as follows. Section II introduces the proposed method for detecting the islanding and the proposed algorithm for calculating the frequency. Section III presents the design of EF sensors and the shielding mechanism for EF sensors' back-end circuit. Section IV verifies the proposed islanding detection method by the numerical simulations on four kinds of overhead lines in Canada, and also by the extensive experiment on a reduced scale model of overhead lines. Finally, Section V concludes the article.

## II. PROPOSED DETECTION METHOD

This section introduces the idea of the proposed islanding detection method and then introduces how to measure and to calculate the voltage frequency. A complete design process of the proposed single-axis EF sensor and its shielding mechanism is presented as well.

### A. Islanding Detection Algorithm

When a conductor is energized, an EF will distribute around the conductor. The EF waveform is identical to the conductor

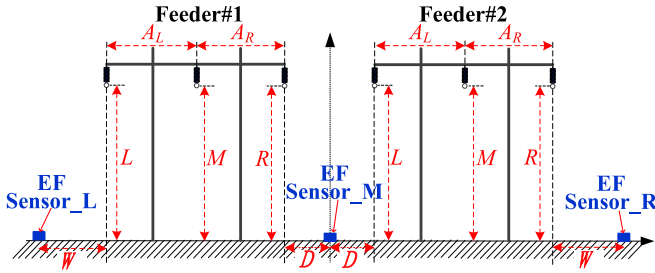


Fig. 2. Schematic of the proposed islanding detection method.

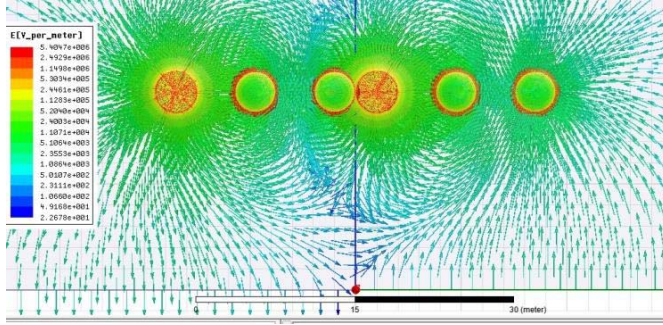


Fig. 3. EF lines of two 240-kV overhead lines. The geometry:  $L = M = R = 18.7$  m;  $A_L = A_R = 7.5$  m;  $D = 2$  m.

voltage waveform. Hence, the conductor voltage frequency can be indirectly calculated by the EF waveform.

The conductor geometry of the existing overhead lines at different voltage levels may be various, but the conductors of the lines are usually arranged in two types: a horizontal line or a triangle line. The diagram of the proposed islanding detection method is shown in Fig. 2.  $A_L$  denotes a horizontal distance between the left conductor and the middle conductor;  $A_R$  denotes the horizontal distance between the middle conductor and the right conductor.  $L$ ,  $M$ , and  $R$  represent the heights of the left, middle, and right conductors, respectively.  $D$  represents the shortest horizontal distance between the EF Sensor\_M and each feeder.  $W$  represents the minimum horizontal distance between the Feeder#1 and the EF Sensor\_L and the minimum horizontal distance between the Feeder#2 and the EF Sensor\_R. The small, portable EF sensors are deployed on the ground and are arranged in a linear array being orthogonal to the axis of the measured feeders. Fig. 3 shows the EF lines of two 240-kV feeders, which are simulated by a commercial finite element method (FEM) software, ANSYS Maxwell. As it can be seen from Fig. 3, the EF lines are perpendicular to the surface of the earth due to the effect of conducting earth plane. Note that only the vertical-direction EF exists in the ground level. Therefore, only the single-axis EF sensors can meet the EF measurement requirement.

Fig. 4 shows the proposed algorithm for the proposed islanding detection method. The indicator of the islanding/nonislanding situation is based on the frequency measurement from three EF sensors. The sensor on the left-hand side (EF Sensor\_L) measures the frequency of Feeder#1. The sensor on the right-hand side (EF Sensor\_R) monitors the frequency of Feeder#2. The sensor in the middle (EF Sensor\_M) confirms the detection results in case of any dysfunctions.

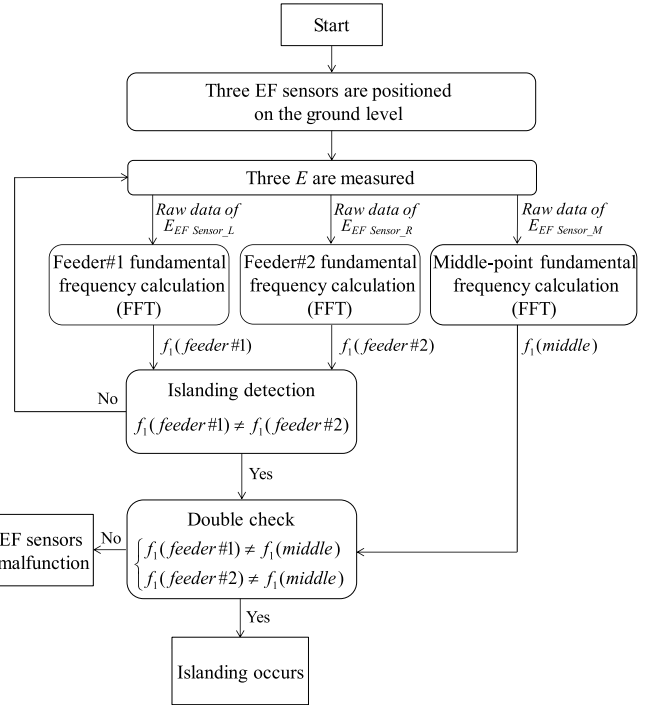


Fig. 4. Proposed algorithm for islanding detection.

functions as a supportive confirmation for the islanding detection process. EF Sensor\_M measures the frequency of the ground-level EF at the middle point. If no islanding occurs, voltages measured by EF Sensor\_L and EF Sensor\_R are synchronous. Hence, values and changes of both voltage frequencies are the same. Moreover, values and changes of the frequency measured by EF Sensor\_M will be the same as that measured by the other two sensors. In the real scenarios, a transient phenomenon with short or long duration may occasionally affect the voltage frequencies. If no islanding occurs, the three EF sensors (EF Sensor\_L, EF Sensor\_M, and EF Sensor\_R) will also capture the same frequency changes in both interconnected feeders caused by the transient phenomenon. When an islanding occurs, the voltages measured by EF Sensor\_L and EF\_Sensor\_R will be asynchronous. Hence, values and changes of the frequencies measured by EF Sensor\_L and EF Sensor\_R will not be identical anymore. It can be interpreted as that Feeder#1 and Feeder#2 will generate two EFs with similar magnitudes but different frequencies at the position of EF Sensor\_M. EF\_Sensor\_M will capture this difference, which could be understood as a voltage frequency deviation between Feeder#1 and Feeder#2. Note that the waveform at the middle point (EF Sensor\_M) fluctuates dramatically when the islanding is happening, it is very hard to numerically calculate the frequency of the superposition of two EFs. In a word, the measurement from EF Sensor\_L and EF Sensor\_R helps to identify the islanding situation. EF Sensor\_M confirms the detection results in case of any dysfunctions.

#### B. Frequency Calculation Algorithm

It is assumed that the voltage profiles on both the main grid side and DGs side are perfectly synchronized in

a nonislanding situation. When a fault occurs on the main grid side, the protective relay will disconnect the distributed resources from the main power grid. The distribution system is supposed to operate in an islanding mode. All connected loads in this distribution system would be balanced only by DGs. The switching devices of DGs will cause dramatic disturbance, which is detected readily and immediately. The disturbance has two unique patterns: 1) transient state and 2) steady state. Regarding the frequency calculation at the transient state, the advanced commercial power-related software mainly estimates the transient-state frequency in a period of 0.2 s or 0.5 s. Moreover, as the definition in IEC 61000-4-7, a nominal data window requires 12 complete power cycles (approximately 0.2 s) to attain the minimum errors in frequency analysis [71]. This study calculates the voltage frequency every 0.2 s to ensure an accurate measurement during the transient state. Besides, the digital sampling rate of EF sensors is 30 720 samples/s.

The commonly accepted frequency analysis methods for power systems are mainly based on Fourier transform (FT) [72] or zero-crossing time interval determination [73]. FT is called the frequency domain representation of signals. A technology decomposes an original signal into a superposition of sinusoids with specific frequencies. A companion technology of FT, called Short-time FT (STFT), adds a window function on FT and analyzes the sinusoidal frequency within this window as it varies over time. The method, zero-crossing time interval determination, calculates the fundamental frequency by counting the number of completing signal cycles within a selected period. The frequency calculation method defined in IEC 61000-4-30 is based on the zero-crossing time interval determination [74]. This method counts the number of the entire signal cycles during the period of 10 s for the frequency reading.

In this study, EF sensors are used to capture the EFs and are placed under the measured feeders. However, the distribution of the EF over the ground is sensitive to and is easily affected by the ambient environment around the feeders. One of the dominated factors is the electric conductivity of the ground. For example, the melting snow will change the soil humidity, immediately reflecting on a dynamic charging distribution over ground. The dc level of the measured EFs is sensitive to the dynamics of the charging distribution over ground. It is worth to notice that the frequency calculation using the zero-crossing time interval determination is not applicable for this study. Since the changes of dc level of EF will not affect the accuracy of FT. This study chooses FT to analyze the feeders' frequency. The fast FT (FFT) is a distinctive technique which has high computational efficiency. In order to reduce the spectral leakage, a Hanning window is adopted with FFT to calculate the frequency in this study. The adopted frequency calculation algorithm will be tested in Section II-D with the data measured by the proposed EF sensors.

### C. EF Sensor Design

In this study, the new contactless voltage frequency measurement technology for overhead lines has five essential

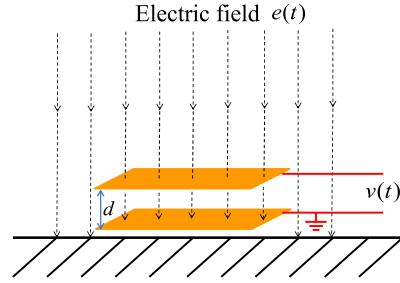


Fig. 5. Drawing of single-axis EF sensor.

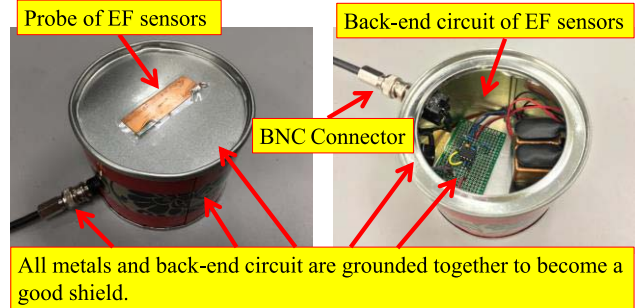


Fig. 6. Photographs of the proposed EF sensor.

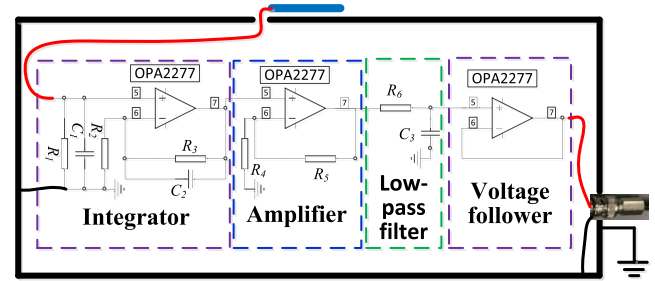


Fig. 7. Circuit diagram of the proposed EF sensor.

features: 1) easy installation; 2) portability; 3) no physical contact for a long-distance measurement; 4) applicability for the overhead-line voltage measurement; and 5) utility assistance free. To achieve these features, a single-axis EF sensor is designed to support the proposed algorithm for conducting an efficient and reliable onsite frequency measurement.

A simple drawing of the single-axis EF sensor is shown in Fig. 5. Since the EF lines are perpendicular to the surface of the earth, the single-axis EF sensor located near the ground level is enough to measure the vertical-direction EF. The single-axis EF sensor is a single capacitor plate which consists of two paralleled plates. In the actual EF measurements, the surfaces of two paralleled plates should be arranged perpendicularly to the EF lines as shown in Fig. 5. The proposed single-axis EF sensor is built on a single capacitor plate in Fig. 6. The shielding structure isolates the back-end circuit from the measured EFs. The shielding structure also isolates the sensing probe from the EFs generated by the back-end circuit. The diagrams of the sensing probe and the back-end circuit are shown in Fig. 7. This design grounds the following components all together: the lower plate of

EF sensor probe, the whole shielding structure, the back-end circuit, and the Bayonet Neill-Concelman (BNC) connector. This design prevents the outputs of the sensing probe from being interfered by other EFs. The back-end circuit mainly consists of an integrator, an amplifier, a low-pass filter, and a voltage follower. The details of EF sensor design rules and working principles are introduced as follows.

The probe of EF sensors can be regarded as a classic parallel-plate capacitor. The paralleled plates are placed close to an energized conductor, the capacitance of the parallel-plate capacitor,  $c$ , is given as a function of its structure geometry

$$c = \epsilon_0 \frac{A}{d} \quad (1)$$

where  $\epsilon_0$  is the electric permittivity of vacuum,  $A$  is the plate surface area of the parallel-plate capacitor, and  $d$  is the distance between two plates.

Assuming the EF  $e(t)$  is uniform between two plates of the parallel-plate capacitor, the electric potential across the capacity is given as

$$v(t) = e(t)d \quad (2)$$

where  $e(t) = E \sin(\omega t)$ , and  $\omega$  is  $2\pi f$ .

A capacitor  $C_1$  and a resistor  $R_1$  are connected to the output of the EF-sensor probe in parallel, as shown in Fig. 7. The paralleled circuit ( $R_1/C_1$ ) and the EF-sensor probe form a loop. The electric current flowing through the parallel-plate capacitor is

$$I = c \frac{dv(t)}{dt}. \quad (3)$$

Substituting (1) into (3), and then expanding (3) as

$$I = \epsilon_0 A \frac{de(t)}{dt} \quad (4)$$

then the voltage across  $C_1$  and  $R_1$  is

$$V_Z = I \frac{R_1}{1 + j\omega C_1 R_1}. \quad (5)$$

In this article, the frequency band is set around the fundamental power frequency (e.g., 60 Hz in Canada). The values of  $R_1$  and  $C_1$  are 1 MΩ and 22 pF, respectively. Hence, (5) can be simplified to

$$V_Z \approx IR_1 = \epsilon_0 A R_1 \frac{de(t)}{dt}. \quad (6)$$

Integrating both sides of (6), and then the EF can be obtained

$$e(t) = \frac{1}{\epsilon_0 A R_1} \int V_Z dt. \quad (7)$$

According to (7), the ground-level EF waveform can be calculated after  $V_Z$  is measured and be processed by the data-acquisition system.

TABLE II  
TEST RESULTS FOR ACCURACY AND RELIABILITY OF PROPOSED EF SENSORS

	Condition	Hz			mHz	
		$f_{ref\_1}^*$ (1st 10 s)	$f_{ref\_2}^+$ (1st 0.2 s)	$f_{sensor}^1$ (1st 0.2 s)	Error <sup>2</sup> (1st 0.2 s)	Standard deviation (1 hr)
EF Sensor_L	55	55.0002	55.0003	55.0003	0.032	0.010
	60	60.0003	60.0003	60.0003	0.042	0.018
	65	65.0003	65.0004	65.0004	0.044	0.015
EF Sensor_M	55	55.0002	55.0003	55.0003	-0.011	0.013
	60	60.0003	60.0004	60.0004	-0.013	0.014
	65	65.0003	65.0004	65.0004	-0.011	0.013
EF Sensor_R	55	55.0002	55.0003	55.0003	0.022	0.016
	60	60.0003	60.0004	60.0004	0.011	0.012
	65	65.0003	65.0004	65.0004	0.015	0.017

\* $f_{ref\_1}$ : frequency standard using the zero-crossing time interval determination with the first 10-s data.

<sup>†</sup> $f_{ref\_2}$ : frequency standard using FFT with the first 0.2-s data.

<sup>1</sup> $f_{sensor}$ : EF sensor using FFT with the first 0.2-s data.

<sup>2</sup>Error:  $f_{sensor} - f_{ref\_2}$

#### D. EF Sensor Test

In this test, the proposed EF sensor is placed in a metal container to test its accuracy and reliability. A 120-V ac voltage source is connected to the end of an electric wire. Another end of this electric wire is placed in the metal container. The container is completely sealed and is directly grounded. Only this electric wire and one coaxial cable can pass through the shell of the metal container. The electric wire is used to produce an EF, and then the EF sensor captures this EF and generates a signal which is delivered to a data-acquisition system through the coaxial cable. This special test design helps to isolate the EF sensor from external EFs. The study chooses three frequencies of the 120-V ac voltage source around the measured frequency band (60 Hz), 55, 60, and 65 Hz, to test the performance of the proposed EF sensors. The test results are presented in Table II, where the two frequency standards ( $f_{ref\_1}$  and  $f_{ref\_2}$ ) are obtained by a voltage probe (Probe Master 4321). Note that  $f_{ref\_1}$  represents the frequency calculated by the first 10 s data using the zero-crossing time interval determination and  $f_{ref\_2}$  represents the frequency calculated by the first 0.2 s data using FFT. Table II lists frequency calculation errors in the first 0.2 s of three EF sensors ( $f_{sensor} - f_{ref\_2}$ ) and the standard deviation of all frequency calculation errors collected in each 0.2-s data within one hour. The standard deviation ( $s$ ) is defined in (8). The measurement results ( $f_{ref\_1}$  versus  $f_{ref\_2}$ ) show that the adopted frequency calculation algorithm (FFT) performs well as the zero-crossing time interval determination which is a standardized method documented in IEC 61000-4-30. Regarding the proposed EF sensor, all frequency errors in the first 0.2 s are less than  $\pm 0.05$  MHz for all conditions, and the standard deviation of errors in one hour is below 0.02 MHz for all conditions. Based on these results, it can be concluded that three proposed EF sensors are validated to achieve sufficiently high accuracy and effectiveness on the frequency measurement

$$\text{Sample standard deviation : } s = \sqrt{\frac{1}{N-1} \sum_{i=1}^N (x_i - \bar{x})^2} \quad (8)$$

TABLE III  
GEOMETRY FOR FOUR KINDS OF OVERHEAD LINES

Voltage level	$L(m)$	$M(m)$	$R(m)$	$A_L(m)$	$A_R(m)$
240 kV	18.7	18.7	18.7	7.5	7.5
144 kV	11.6	14.3	12.8	0.3	3.9
25 kV	11.6	12.2	11.6	1.3	1.3
13.8 kV	8.8	9.3	8.8	0.9	0.9

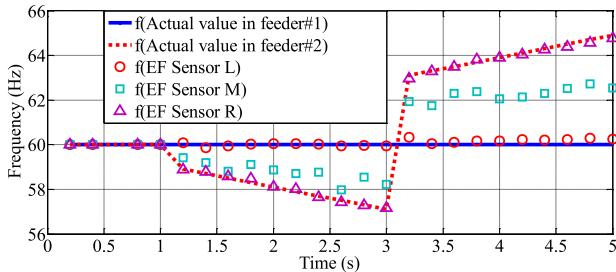


Fig. 8. Frequency dynamics on the 240-kV overhead line. The case varies  $R_f$  values in (9) on Feeder#2 side, in the purpose to generate the frequency disturbance. The  $R_f$  is equal to  $-1$  from  $1$  to  $3$  s, and then changed to  $1$  from  $3$  to  $5$  s.

where  $x_i$  are the errors of the calculated frequencies (using the FFT) at the  $i$ th time interval (time step is  $0.2$  s). The study collected the errors  $x_i$  within one hour, which will come to  $N$  data points of the errors. The  $\bar{x}$  is the mean value of all errors data.

### III. NUMERICAL VERIFICATION

#### A. Simulation Setup

With the reliable EF sensor measurement, this study moves to a feasibility evaluation of the proposed islanding detection on four types of Canadian overhead lines with the different conductor geometry. The structure of overhead lines is shown in Fig. 2. To simplify simulations, the study assumes  $D$  is  $2$  m, and  $W$  is  $5$  m for all these four kinds of overhead lines. The other geometric parameters of these overhead lines are listed in Table III. Regarding the test voltage frequency, the dynamic compliance test in IEEE Standard C37.118.1 [75] is adopted to generate the frequency variation. The voltage is defined in (9), and its frequency change is linear. Moreover, all simulations are done using MATLAB

$$V = V_m \cos(\omega_0 t + \pi R_f t^2) \quad (9)$$

where  $R_f$  (Hz/s) is the ramp rate of the frequency.

#### B. Verification of Frequency Calculation

In this case, only the voltage frequency of Feeder#2 is chosen as a parameter to simulate and to analyze actual conditions. Fig. 8 visualizes the frequency dynamics on the 240-kV overhead line. The initial frequency is  $60$  Hz in the first second. After  $1$  s, the voltage on Feeder#2 by (9) starts to change for simulating the frequency variations. This study also conducts the same simulations for the other three types of overhead lines. The simulation results show that EF Sensor\_L

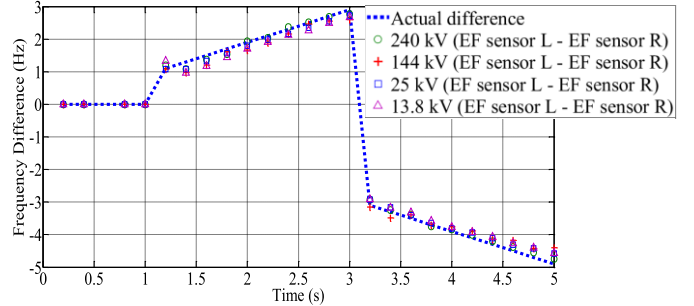


Fig. 9. Measurement validation of the frequency difference between two feeders. The comparison between the actual difference and the measured difference demonstrates the accuracy and the flexibility of the proposed method.

TABLE IV  
MAXIMUM FREQUENCY MEASUREMENT RELATIVE ERRORS  
FOR DIFFERENT LOCATIONS OF EF SENSORS

	$W/D$ ( $D=2$ m)				
	0	1	2.5	3.5	4.5
240 kV	-9.21%	-7.43%	-5.43%	-4.31%	-3.96%
144 kV	-9.69%	-8.70%	-6.84%	-5.29%	-4.76%
25 kV	-9.57%	-8.43%	-6.57%	-5.11%	-4.56%
13.8 kV	-10.16%	-9.96%	-7.95%	-6.29%	-5.23%

and EF Sensor\_R successfully capture the frequency of their measured feeders. EF Sensor\_M measures the superposition of two voltage frequency of Feeder#1 and Feeder#2, which helps to confirm whether an islanding is happening.

Fig. 9 visualizes the frequency difference between two feeders (Feeder#1 and Feeder#2). Note that the plots of the 240, 25, and 13.8 kV cases almost overlap together due to their similar conductor geometry. The 144 kV case shows larger fluctuations, since the three-phase conductors of the 144-kV overhead line are distributed as a triangle, resulting in a smaller EF. In summary, the proposed islanding detection method can accurately and quickly respond to the frequency changes during the real-time operation for different types of overhead lines with a wide range of voltage levels.

#### C. Impact on Parameters $D$ and $W$

The location of EF sensors is a significant factor affecting the measurement results. This section discusses how the EF sensors' placement would impact the measurement results. Note that EF sensors are placed at the position ( $D = 2$  m and  $W = 5$  m) for all types of overhead lines in the previous simulations. Here, the parameter  $D$  is fixed to  $2$  m and  $W/D$  is varied to indicate the different locations of EF sensors, and then redoes the same evaluations, like Section III-B. Table IV provides the largest relative errors of the measured frequency deviations among 25 measurements (each sample in  $5$  s). Note that the case of 13.8-kV overhead line has the most serious EF interference at selected positions ( $W/D$  ratio) of the EF sensor due to the tight arrangement of the six-phase conductors. The largest relative error of the 13.8-kV case when  $W/D = 2.5$

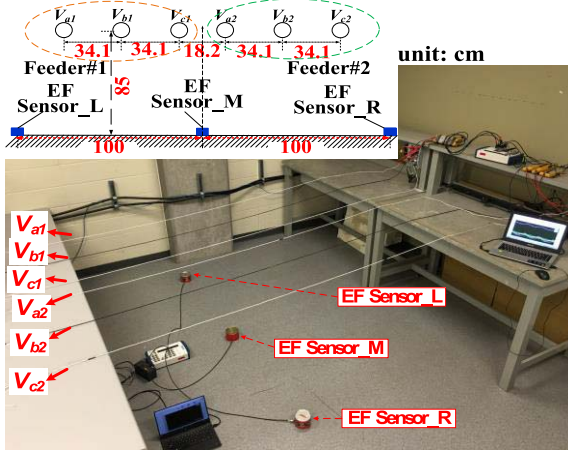


Fig. 10. Measurement system testbed.

is  $-7.95\%$ , which occurs at 1.2 s in Fig. 9. Even given such a large measurement error, the actual and measured frequency differences are 1.1001 and 1.0126 Hz, which is technically acceptable for the purpose of islanding detection. Note that the relative errors of the four kinds of overhead lines decrease dramatically with the increasing  $W/D$ . Since the proposed detection method is designed for the on-site usage, the selected value  $W/D = 2.5$  is adopted in the design. It can be concluded that this relative error will not affect the detection results of the proposed method. Furthermore, the 144-kV case always has larger relative errors than the 25-kV case. The reason is that the 144-kV conductors are arranged in a triangle, but the 25-kV conductors are arranged in a line. When both heights of the 144 kV and the 25-kV overhead lines are similar as listed in Table III, the triangle arrangement of the 144-kV conductors results in a larger EF interference between two feeders.

$$\text{Relative error} = \frac{\text{difference (proposed method)} - \text{actual difference}}{\text{actual difference}} \times 100\%. \quad (10)$$

#### IV. MEASUREMENT RESULTS AND DISCUSSIONS

This section introduces the experiment on a testbed for the validation of 1) frequency response of the proposed EF sensors and 2) detection performance.

##### A. Frequency Response Test for EF Sensors

The proposed testbed consists of two reduced scale overhead lines shown in Fig. 10, namely two feeders. The geometry of the two test feeders is scaled in the same proportions as 240-kV Canadian overhead lines listed in Table III. The rated three-phase voltage is 208 V, and the voltage references are voltage probes (Probe Master 4321). The outputs of three EF sensors are collected by a data-acquisition system consisting of National Instruments-data acquisition (NI-DAQ) card and a laptop. The frequency is calculated by the proposed algorithm in Section II-B. Three scenarios with different load and feeder conditions are shown in Table V. The two settings

TABLE V  
FREQUENCY RESPONSES OF EF SENSORS FOR THREE DIFFERENT KINDS OF FEEDERS' SITUATIONS

	Feeder#1 ( $V_{al}, V_{bl}, V_{cl}$ )	Feeder#2 ( $V_{a2}, V_{b2}, V_{c2}$ )
Case 1	Load condition	No load
	Feeder condition	• Interconnected power system
Case 2	Load condition	No load
	Feeder condition	• Non-interconnected power system • Frequency of Feeder#1 is changed from 59.95 Hz to 60.05 Hz
Case 3	Load condition	No load
	Feeder condition	• Non-interconnected power system • Frequency of Feeder#1 is changed from 59.95 Hz to 60.05 Hz

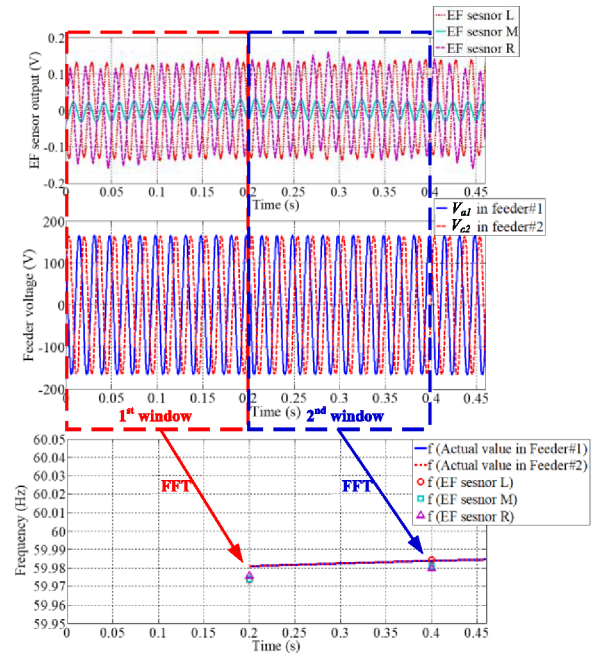


Fig. 11. Waveforms of EF sensors and feeders, and FFT window size of 0.2 s.

of time window for frequency calculation are investigated, i.e., 0.2 and 10 s. Fig. 11 shows the waveforms of three EF sensor outputs and two feeder voltage profiles ( $V_{a1}$  and  $V_{c2}$  as shown in Fig. 10) for the first 0.46-s measurement in Case 1. Moreover, the size of time window is 0.2 s for FFT. Computational steps of the FFT composed in MATLAB consist of 1) defining a Hanning window; 2) using the FFT function; and 3) finding the fundamental frequency. Table VI shows the FFT results for the first two 0.2-s windows. The frequencies of Feeder#1 and Feeder#2 are almost identical, and the frequency measurements from three EF sensors are similar to the frequencies of feeders. Frequency differences between each EF sensor and feeder are within  $\pm 0.01$  Hz. The results demonstrate that even if there is a nonconsistent dc offset in each EF waveform as shown in Fig. 11, the proposed frequency calculation algorithm can perform an accurate frequency measurement, which is very important for realizing the proposed islanding detection method.

TABLE VI  
FFT RESULTS FOR FIRST TWO WINDOWS

	Frequency (Hz)				
	Feeder#1	Feeder#2	EF sensor L	EF sensor M	EF sensor R
1 <sup>st</sup> window	59.9802	59.9801	59.9738	59.9742	59.9765
2 <sup>nd</sup> window	59.9840	59.9839	59.9849	59.9811	59.9802

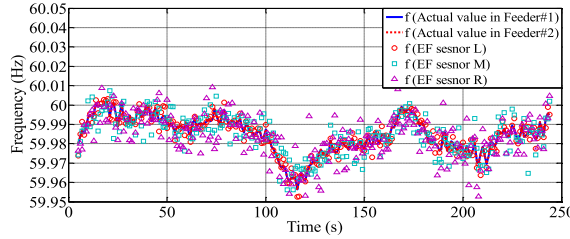


Fig. 12. Case 1: frequency measurement results in every 0.2 s.

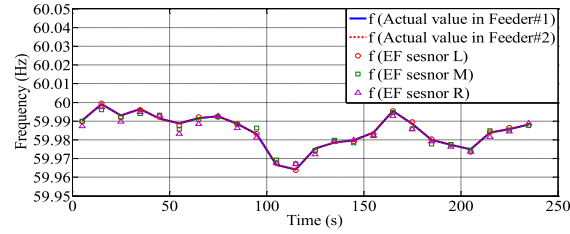


Fig. 13. Case 1: frequency measurement results in every 10 s.

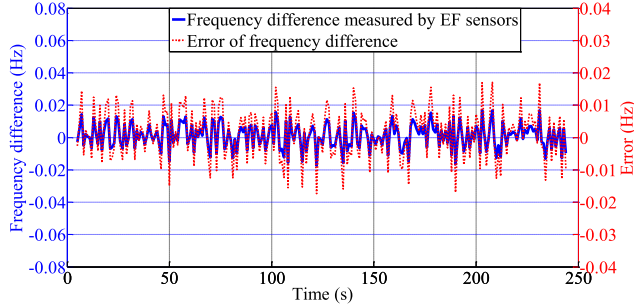


Fig. 14. Case 1: frequency difference of two feeders measured by EF sensors (0.2-s window). The measurement errors are bounded by  $\pm 0.02$  Hz.

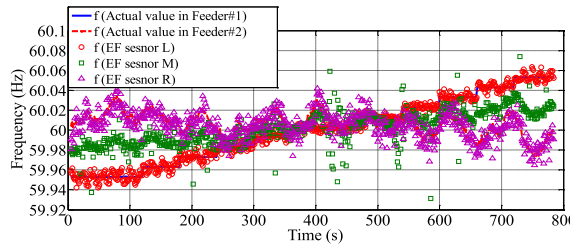


Fig. 15. Case 2: frequency measurement results in every 0.2 s.

The whole measurement results for Cases 1–3 in Table V are shown in Figs. 12–20.

In Case 1, the two feeders are interconnected and are grid-connected, and the results in Figs. 12 and 13 show that the two frequencies measured by EF Sensor\_L and EF Sensor\_R are

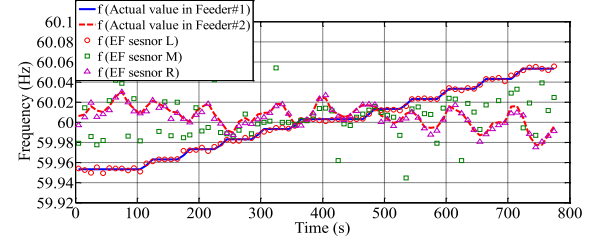


Fig. 16. Case 2: frequency measurement results in every 10 s.

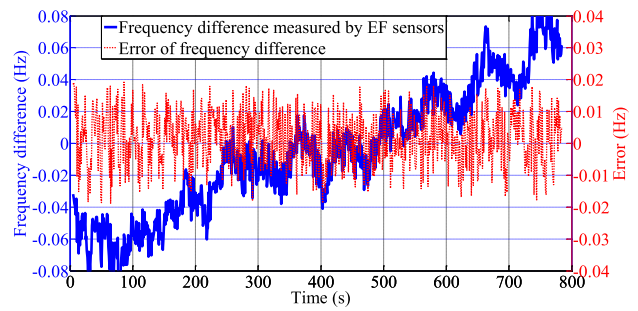


Fig. 17. Case 2: frequency difference of two feeders measured by EF sensors (0.2-s window). The measurement errors are bounded by  $\pm 0.02$  Hz.

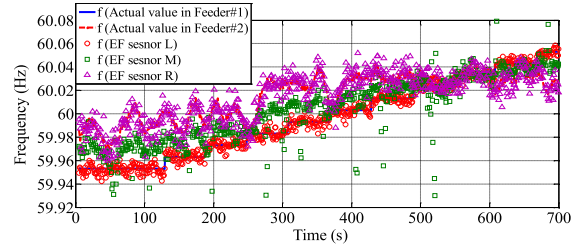


Fig. 18. Case 3: frequency measurement results in every 0.2 s.

the same as the actual voltage frequency. EF Sensor\_M provides a nonislanding confirmation. Fig. 14 shows the frequency differences between two feeders measured by EF sensors (EF Sensor\_L and EF Sensor\_R) and the corresponding measurement errors. It is clear to see that the maximum errors are located within  $\pm 0.02$  Hz.

In Case 2, the two feeders are not interconnected. Only Feeder#2 is grid-connected, but the frequency of Feeder#1 is increased from 59.95 to 60.05 Hz with 0.01-Hz step size. The measurement results in Figs. 15 and 16 show that EF Sensor\_L can immediately and explicitly capture the frequency variations from 59.95 to 60.05 Hz; meanwhile, a superposition of frequency is measured by EF Sensor\_M, which fluctuates dramatically. Fig. 17 shows the frequency differences between two feeders measured by EF sensors. The maximum measurement errors are also located within  $\pm 0.02$  Hz.

In Case 3, the feeder setup is the same as that in Case 2, but different kinds of loads are added onto Feeder#2. It can be seen from Figs. 18 and 19 that EF Sensor\_L still immediately responds to the frequency variations from 59.95 to 60.05 Hz, and EF Sensor\_R also accurately and timely indicates the frequency when Feeder#2's load is time varying. Fig. 20 shows the frequency differences between two feeders measured by

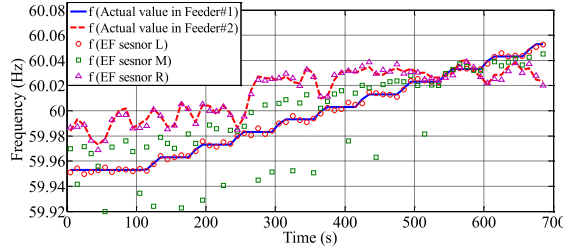


Fig. 19. Case 3: frequency measurement results in every 10 s.

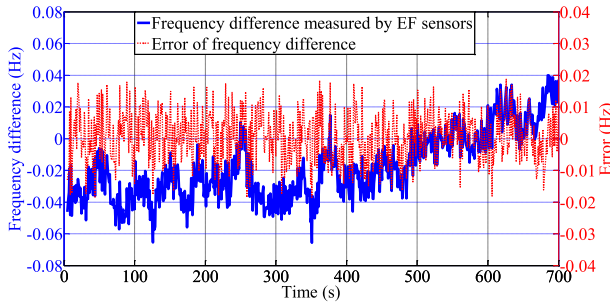


Fig. 20. Case 3: frequency difference of two feeders measured by EF sensors (0.2-s window). The measurement errors are bounded by  $\pm 0.02$  Hz.

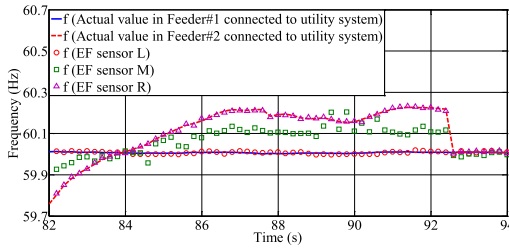


Fig. 21. Frequency measurement results in a period of 0.2 s when the synchronous generator starts and then is connected to the utility system.

EF sensors, and the maximum measurement errors are still located within  $\pm 0.02$  Hz, which is considered as an acceptable performance.

In a summary, based on the frequency response analysis of the proposed EF sensor in Figs. 12–20, the performance of the proposed frequency calculation algorithm with a designed EF sensor can guarantee the measurement accuracy (e.g., errors bounded within  $\pm 0.02$  Hz) in various kinds of feeders and load settings.

### B. Islanding Detection Test

In this section, an onsite islanding detection experiment is conducted on the testbed as shown in Fig. 10. To test the feasibility of the proposed method, the study connects a three-phase 208 V/10 kW synchronous generator to Feeder#2. Feeder#1 is connected to the utility system at the rated voltage of 208 V. The synchronous generator operates in two phases: interconnect or dis-interconnected with the utility system. The transient-state frequencies in these two phases are calculated and analyzed. In Fig. 21, it can be seen that when the synchronous generator starts and then is connected to the utility system at around 92.5 s, EF Sensor\_R can accurately measure

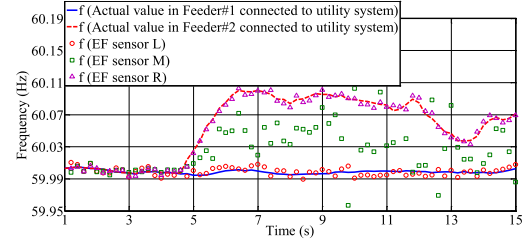


Fig. 22. Frequency measurement results in a period of 0.2 s when an island occurs.

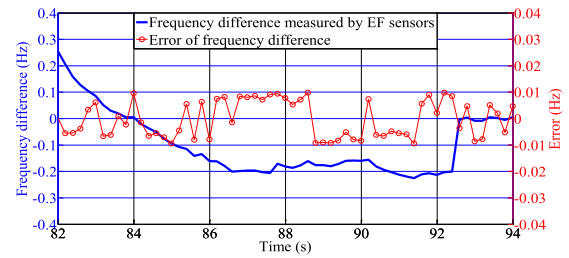


Fig. 23. Frequency difference of two feeders measured by EF sensors. The measurement errors are bounded by  $\pm 0.01$  Hz. The synchronous generator (Feeder#2) is connected to the utility system at the time 92.5 s.

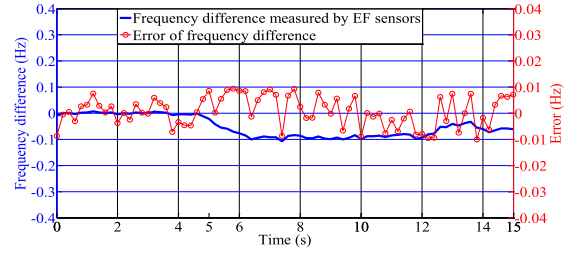


Fig. 24. Frequency difference of two feeders measured by EF sensors. The measurement errors are bounded by  $\pm 0.01$  Hz. The synchronous generator (Feeder#2) is disconnected from the utility system at the time 4.5 s.

the frequency change on Feeder#2. In Fig. 22, the results show that when an islanding occurs, namely, the generator is disconnected from the utility system at around 4.5 s, EF Sensor\_R can immediately measure the transient-state frequency, and EF Sensor\_M also instantly indicates the superposition of two different frequencies. Hence, EF Sensor\_M characterizes an assisting identification index in islanding detection. It is concluded that the proposed method can precisely detect the frequency features between islanding and nonislanding situations. The frequency measurements from three EF sensors are dependable for the islanding classification. Figs. 23 and 24 show the frequency difference between two feeders and the corresponding measurement errors. The measurement errors are bounded within  $\pm 0.01$  Hz. Figs. 23 and 24 demonstrate that the proposed islanding detection method is supported by a reliable frequency measurement tool (EF sensor) and a well-designed calculation algorithm.

## V. CONCLUSION

A new contactless islanding detection method has been proposed in this article. In the proposed method, only three

single-axis EF sensors are placed on the ground to measure EFs of overhead lines. With a frequency calculation algorithm, the proposed islanding detection can be easily carried out in practice by measuring the voltage frequency deviations. This study conducted numerical simulations of four different voltage-level overhead lines to demonstrate the feasibility of proposed islanding detection method. The experiment results also show the proposed method can accurately measure the voltage frequency of the overhead line. In the frequency response test for designed EF sensors, the largest measurement error is only approximately 0.02 Hz. In the islanding detection test on the testbed, the largest measurement error is only approximately 0.01 Hz. It is expected that the proposed method can be easily extended to a wide range of overhead lines by parameterizing the frequency threshold value based on grid properties and characteristics of DGs.

The main contributions of this research work are concluded as follows: 1) proposed contactless islanding detection method addresses several challenges of the onsite islanding detection; 2) proposed method is low cost-efficiency. Three single-axis EF sensors successfully ensure an accurate and reliable detection; 3) structure of the proposed single-axis EF sensor is simple. The critical component, a single capacitor plate with a shield structure, is easy to obtain and to assemble; 4) reliable detection is ensured by a carefully designed EF sensors structure for avoiding any dysfunctions of any EF sensors; 5) proposed method is designed for engineers' convenience and safety; and 6) proposed method has potentials and advantages to replace the traditional current transformers (CTs) for the field measurement with the concerns over the cost, portability, safety, stability, and reliability.

Future works enabled by this research are identified as follows.

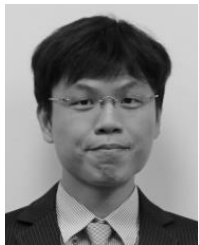
- 1) The proposed algorithm is only suitable for the islanding detection for two feeders, which is as shown in Fig. 1. In the future stages, the proposed algorithm can be improved to differentiate faults and abrupt load changes based on solutions, which have been used in the existing passive methods.
- 2) The proposed method can be specified in microgrids with multiple DGs and distribution systems with multi-feeders for the islanding detections.
- 3) Future investigation can also be focused on how to avoid the NDZ during low or zero power imbalance condition, which is commonly recognized as a limitation in the existing passive islanding detection techniques.
- 4) The performance of the proposed method can be compared with the existing detection method using numerical simulations.
- 5) Additional on-site experiment on real overhead lines is necessary for validating the feasibility of the proposed method as field measurements. In the future stages, overhead lines with different geometry will be investigated to extend the proposed method to other field measurements.

## REFERENCES

- [1] G. Artale *et al.*, "Smart interface devices for distributed generation in smart grids: The case of islanding," *IEEE Sensors J.*, vol. 17, no. 23, pp. 7803–7811, Dec. 2017.
- [2] A. V. Soumya and J. B. Edward, "Review of islanding detection techniques for distributed energy sources," *Int. J. Adv. Res. Sci., Eng. Technol.*, vol. 3, no. 3, pp. 135–138, Aug. 2016.
- [3] W. Xu, G. Zhang, C. Li, W. Wang, G. Wang, and J. Kliber, "A power line signaling based technique for anti-islanding protection of distributed generators—Part I: Scheme and analysis," *IEEE Trans. Power Del.*, vol. 22, no. 3, pp. 1758–1766, Jul. 2007.
- [4] A. Cataliotti *et al.*, "A prototypal architecture of a IEEE 21451 network for smart grid applications based on power line communications," *IEEE Sensors J.*, vol. 15, no. 5, pp. 2460–2467, May 2015.
- [5] S. Rinaldi *et al.*, "Characterization of IP-based communication for smart grid using software-defined networking," *IEEE Trans. Instrum. Meas.*, vol. 67, no. 10, pp. 2410–2419, Oct. 2018.
- [6] P. Kundu and A. K. Pradhan, "Supervisory protection of islanded networks using synchrophasor data," *IEEE Trans. Smart Grid*, vol. 10, no. 2, pp. 1772–1780, Mar. 2019.
- [7] P. Gopakumar, M. J. B. Reddy, and D. K. Mohanta, "Phasor measurement sensor-based angular stability retention system for smart power grids with high penetration of microgrids," *IEEE Sensors J.*, vol. 18, no. 2, pp. 764–772, Jan. 2018.
- [8] J. Stevens, R. Bonn, J. Ginn, S. Gonzalez, and G. Kern, "Development and testing of an approach to anti-islanding in utility-interconnected photovoltaic systems," Sandia Nat. Lab., Albuquerque, NM, USA, Tech. Rep. SAND2000-1939, Aug. 2000.
- [9] H. Karimi, A. Yazdani, and R. Iravani, "Negative-sequence current injection for fast islanding detection of a distributed resource unit," *IEEE Trans. Power Electron.*, vol. 23, no. 1, pp. 298–307, Jan. 2008.
- [10] W. Cai, B. Liu, S. Duan, and C. Zou, "An islanding detection method based on dual-frequency harmonic current injection under grid impedance unbalanced condition," *IEEE Trans. Ind. Informat.*, vol. 9, no. 2, pp. 1178–1187, May 2013.
- [11] L. A. C. Lopes and H. Sun, "Performance assessment of active frequency drifting islanding detection methods," *IEEE Trans. Energy Convers.*, vol. 21, no. 1, pp. 171–180, Mar. 2006.
- [12] P. Du, Z. Ye, E. E. Aponte, J. K. Nelson, and L. Fan, "Positive-feedback-based active anti-islanding schemes for inverter-based distributed generators: Basic principle, design guideline and performance analysis," *IEEE Trans. Power Electron.*, vol. 25, no. 12, pp. 2941–2948, Dec. 2010.
- [13] A. M. I. Mohamad and Y. A.-R.-I. Mohamed, "Analysis and mitigation of interaction dynamics in active DC distribution systems with positive feedback islanding detection schemes," *IEEE Trans. Power Electron.*, vol. 33, no. 3, pp. 2751–2773, Mar. 2018.
- [14] M. A. Hosani, Z. Qu, and H. H. Zeineldin, "Scheduled perturbation to reduce nondetection zone for low gain sandia frequency shift method," *IEEE Trans. Smart Grid*, vol. 6, no. 6, pp. 3095–3103, Nov. 2015.
- [15] H. Vahedi, M. Karrari, and G. B. Gharehpetian, "Accurate SFS parameter design criterion for inverter-based distributed generation," *IEEE Trans. Power Del.*, vol. 31, no. 3, pp. 1050–1059, Jun. 2016.
- [16] F. Liu, Y. Kang, Y. Zhang, S. Duan, and X. Lin, "Improved SMS islanding detection method for grid-connected converters," *IET Renew. Power Gener.*, vol. 4, no. 1, pp. 36–42, Jan. 2010.
- [17] M. Liu, W. Zhao, S. Huang, Q. Wang, and K. Shi, "Problems in the classic frequency shift islanding detection methods applied to energy storage converters and a coping strategy," *IEEE Trans. Energy Convers.*, vol. 33, no. 2, pp. 496–505, Jun. 2018.
- [18] H. Vahedi and M. Karrari, "Adaptive fuzzy sandia frequency-shift method for islanding protection of inverter-based distributed generation," *IEEE Trans. Power Del.*, vol. 28, no. 1, pp. 84–92, Jan. 2013.
- [19] S. Bifaretti, A. Lidozzi, L. Solero, and F. Crescimbini, "Anti-islanding detector based on a robust PLL," *IEEE Trans. Ind. Appl.*, vol. 51, no. 1, pp. 398–405, Jan./Feb. 2015.
- [20] Q. Sun, J. M. Guerrero, T. Jing, J. C. Vasquez, and R. Yang, "An islanding detection method by using frequency positive feedback based on FLL for single-phase microgrid," *IEEE Trans. Smart Grid*, vol. 8, no. 4, pp. 1821–1830, Jul. 2017.
- [21] P. Gupta, R. S. Bhatia, and D. K. Jain, "Average absolute frequency deviation value based active islanding detection technique," *IEEE Trans. Smart Grid*, vol. 6, no. 1, pp. 26–35, Jan. 2015.
- [22] G.-K. Hung, C.-C. Chang, and C.-L. Chen, "Automatic phase-shift method for islanding detection of grid-connected photovoltaic inverters," *IEEE Trans. Energy Convers.*, vol. 18, no. 1, pp. 169–173, Mar. 2003.
- [23] F. Briz, D. Diaz-Reigosa, C. Blanco, and J. M. Guerrero, "Coordinated operation of parallel-connected inverters for active islanding detection using high-frequency signal injection," *IEEE Trans. Ind. Appl.*, vol. 50, no. 5, pp. 3476–3484, Sep./Oct. 2014.

- [24] K. Jia, H. Wei, T. Bi, D. W. P. Thomas, and M. Sumner, "An islanding detection method for multi-DG systems based on high-frequency impedance estimation," *IEEE Trans. Sustain. Energy*, vol. 8, no. 1, pp. 74–83, Jan. 2017.
- [25] X. Chen and Y. Li, "An islanding detection method for inverter-based distributed generators based on the reactive power disturbance," *IEEE Trans. Power Electron.*, vol. 31, no. 5, pp. 3559–3574, May 2016.
- [26] P. Gupta, R. S. Bhatia, and D. K. Jain, "Active ROCOF relay for islanding detection," *IEEE Trans. Power Del.*, vol. 32, no. 1, pp. 420–429, Feb. 2017.
- [27] S. Dhar and P. K. Dash, "Adaptive threshold based new active islanding protection scheme for multiple PV based microgrid application," *IET Gener. Transmiss. Distrib.*, vol. 11, no. 1, pp. 118–132, Jan. 2017.
- [28] S. Park, M. Kwon, and S. Choi, "Reactive power P&O anti-islanding method for a grid-connected inverter with critical load," *IEEE Trans. Power Electron.*, vol. 34, no. 1, pp. 204–212, Jan. 2019.
- [29] R. Nale and M. Biswal, "Comparative assessment of passive islanding detection techniques for microgrid," in *Proc. Int. Conf. Innov. Inf. Embedded Commun. Syst. (ICIECS)*, Coimbatore, India, Mar. 2017, pp. 1–5.
- [30] H. H. Zeineldin and J. L. Kirtley, "Performance of the OVP/UVP and OFP/UFP method with voltage and frequency dependent loads," *IEEE Trans. Power Del.*, vol. 24, no. 2, pp. 772–778, Apr. 2009.
- [31] B. Singam and L. Y. Hui, "Assessing SMS and PJD schemes of anti-islanding with varying quality factor," in *Proc. IEEE Int. Power Energy Conf.*, Putrajaya, Malaysia, Nov. 2006, pp. 196–201.
- [32] W. Freitas, W. Xu, C. M. Affonso, and Z. Huang, "Comparative analysis between ROCOF and vector surge relays for distributed generation applications," *IEEE Trans. Power Del.*, vol. 20, no. 2, pp. 1315–1324, Apr. 2005.
- [33] S.-I. Jang and K.-H. Kim, "An islanding detection method for distributed generations using voltage unbalance and total harmonic distortion of current," *IEEE Trans. Power Del.*, vol. 19, no. 2, pp. 745–752, Apr. 2004.
- [34] A. Samui and S. R. Samantaray, "Assessment of ROCPAD relay for islanding detection in distributed generation," *IEEE Trans. Smart Grid*, vol. 2, no. 2, pp. 391–398, Jun. 2011.
- [35] F.-S. Pai and S.-J. Huang, "A detection algorithm for islanding-prevention of dispersed consumer-owned storage and generating units," *IEEE Trans. Energy Convers.*, vol. 16, no. 4, pp. 346–351, Dec. 2001.
- [36] G. Marchesan, M. R. Muraro, G. Cardoso, L. Mariotto, and A. P. de Moraes, "Passive method for distributed-generation island detection based on oscillation frequency," *IEEE Trans. Power Del.*, vol. 31, no. 1, pp. 138–146, Feb. 2016.
- [37] S. K. Salman, D. J. King, and G. Weller, "New loss of mains detection algorithm for embedded generation using rate of change of voltage and changes in power factors," in *Proc. 7th Int. Conf. Develop. Power Syst. Protection (DPSP)*, Amsterdam, The Netherlands, Apr. 2001, pp. 82–85.
- [38] M. R. Alam, K. M. Muttaqi, and A. Bouzerdoum, "A multifeature-based approach for islanding detection of DG in the subcritical region of vector surge relays," *IEEE Trans. Power Del.*, vol. 29, no. 5, pp. 2349–2358, Oct. 2014.
- [39] D. D. Reigosa, F. Briz, C. B. Charro, and J. M. Guerrero, "Passive islanding detection using inverter nonlinear effects," *IEEE Trans. Power Electron.*, vol. 32, no. 11, pp. 8434–8445, Nov. 2017.
- [40] K. Colombage, J. Wang, C. Gould, and C. Liu, "PWM harmonic signature-based islanding detection for a single-phase inverter with PWM frequency hopping," *IEEE Trans. Ind. Appl.*, vol. 53, no. 1, pp. 411–419, Jan./Feb. 2017.
- [41] N. Gupta and R. Garg, "Algorithm for islanding detection in photovoltaic generator network connected to low-voltage grid," *IET Gener. Transmiss. Distrib.*, vol. 12, no. 10, pp. 2280–2287, May 2018.
- [42] R. Nale, M. Biswal, and N. Kishor, "A transient component based approach for islanding detection in distributed generation," *IEEE Trans. Sustain. Energy*, vol. 10, no. 3, pp. 1129–1138, Jul. 2019.
- [43] V. Menon and M. H. Nehrir, "A hybrid islanding detection technique using voltage unbalance and frequency set point," *IEEE Trans. Power Syst.*, vol. 22, no. 1, pp. 442–448, Feb. 2007.
- [44] P. Mahat, Z. Chen, and B. Bak-Jensen, "A hybrid islanding detection technique using average rate of voltage change and real power shift," *IEEE Trans. Power Del.*, vol. 24, no. 2, pp. 764–771, Apr. 2009.
- [45] M. Khodaparastan, H. Vahedi, F. Khazaeli, and H. Oraee, "A novel hybrid islanding detection method for inverter-based DGs using SFS and ROCOF," *IEEE Trans. Power Del.*, vol. 32, no. 5, pp. 2162–2170, Oct. 2017.
- [46] S. D. Kermany, M. Joorabian, S. Deilami, and M. A. S. Masoum, "Hybrid islanding detection in microgrid with multiple connection points to smart grids using fuzzy-neural network," *IEEE Trans. Power Syst.*, vol. 32, no. 4, pp. 2640–2651, Jul. 2017.
- [47] F. Namdari, M. Parvizi, and E. Rokrok, "A new hybrid islanding detection method combination of NJSMS and Q-f for islanding detection of microgrids," in *Proc. 9th Power Syst. Protection Control Conf. (PSPC)*, Tehran, Iran, Jan. 2015, pp. 6–11.
- [48] O. Raipala, A. Mäkinen, S. Repo, and P. Jarventausta, "An anti-islanding protection method based on reactive power injection and ROCOF," *IEEE Trans. Power Del.*, vol. 32, no. 1, pp. 401–410, Feb. 2017.
- [49] A. Samui and S. R. Samantaray, "Wavelet singular entropy-based islanding detection in distributed generation," *IEEE Trans. Power Del.*, vol. 28, no. 1, pp. 411–418, Jan. 2013.
- [50] H. T. Do, X. Zhang, N. V. Nguyen, S. S. Li, and T. T.-T. Chu, "Passive-islanding detection method using the wavelet packet transform in grid-connected photovoltaic systems," *IEEE Trans. Power Electron.*, vol. 31, no. 10, pp. 6955–6967, Oct. 2016.
- [51] S. A. Saleh, R. Meng, R. McSheffery, S. E. Buck, and E. Ozkop, "Performance of multiframe digital interconnection protection for distributed cogeneration systems," *IEEE Trans. Ind. Appl.*, vol. 54, no. 2, pp. 1166–1181, Mar./Apr. 2018.
- [52] P. K. Ray, N. Kishor, and S. R. Mohanty, "Islanding and power quality disturbance detection in grid-connected hybrid power system using wavelet and S-transform," *IEEE Trans. Smart Grid*, vol. 3, no. 3, pp. 1082–1094, Sep. 2012.
- [53] M. Mishra, M. Sahani, and P. K. Rout, "An islanding detection algorithm for distributed generation based on Hilbert–Huang transform and extreme learning machine," *Sustain. Energy, Grids Netw.*, vol. 9, pp. 13–26, Mar. 2017.
- [54] D. Montenegro, G. A. Ramos, and S. Bacha, "An iterative method for detecting and localizing islands within sparse matrixes using DSSim-RT," *IEEE Trans. Ind. Appl.*, vol. 54, no. 1, pp. 675–684, Jan./Feb. 2018.
- [55] M. Bakhshi, R. Noroozian, and G. B. Gharehpetian, "Novel islanding detection method for multiple DGs based on forced Helmholtz oscillator," *IEEE Trans. Smart Grid*, vol. 9, no. 6, pp. 6448–6460, Nov. 2018.
- [56] N. B. Hartmann, R. C. D. Santos, A. P. Grilo, and J. C. M. Vieira, "Hardware implementation and real-time evaluation of an ANN-based algorithm for anti-islanding protection of distributed generators," *IEEE Trans. Ind. Electron.*, vol. 65, no. 6, pp. 5051–5059, Jun. 2018.
- [57] B. Matic-Cuka and M. Kezunovic, "Islanding detection for inverter-based distributed generation using support vector machine method," *IEEE Trans. Smart Grid*, vol. 5, no. 6, pp. 2676–2686, Nov. 2014.
- [58] Q. Cui, K. El-Arroudi, and G. Joós, "Islanding detection of hybrid distributed generation under reduced non-detection zone," *IEEE Transactions on Smart Grid*, vol. 9, no. 5, pp. 5027–5037, Sep. 2018.
- [59] O. N. Faqhruldin, E. F. El-Saadany, and H. H. Zeineldin, "A universal islanding detection technique for distributed generation using pattern recognition," *IEEE Trans. Smart Grid*, vol. 5, no. 4, pp. 1985–1992, Jul. 2014.
- [60] S. Dhar and P. K. Dash, "Harmonic profile injection-based hybrid active islanding detection technique for PV-VSC-based microgrid system," *IEEE Trans. Sustain. Energy*, vol. 7, no. 4, pp. 1473–1481, Oct. 2016.
- [61] D. Mlakic, H. R. Baghaee, and S. Nikolovski, "A novel ANFIS-based islanding detection for inverter-interfaced microgrids," *IEEE Trans. Smart Grid*, vol. 10, no. 4, pp. 4411–4424, Jul. 2019.
- [62] A. Khamis, Y. Xu, Z. Y. Dong, and R. Zhang, "Faster detection of microgrid islanding events using an adaptive ensemble classifier," *IEEE Trans. Smart Grid*, vol. 9, no. 3, pp. 1889–1899, May 2018.
- [63] F. Xue, J. Hu, S. X. Wang, and J. He, "Electric field sensor based on piezoelectric bending effect for wide range measurement," *IEEE Trans. Ind. Electron.*, vol. 62, no. 9, pp. 5730–5737, Sep. 2015.
- [64] C. A. Gerrand, J. R. Gibson, G. R. Jones, L. Holt, and D. Simkin, "Measurements of power system voltages using remote electric field monitoring," *IEE Proc.-Gener., Transmiss. Distrib.*, vol. 145, no. 3, pp. 217–224, May 1998.
- [65] K. Zhu, W. K. Lee, and P. W. T. Pong, "Non-contact capacitive-coupling-based and magnetic-field-sensing-assisted technique for monitoring voltage of overhead power transmission lines," *IEEE Sensors J.*, vol. 17, no. 4, pp. 1069–1083, Feb. 2017.
- [66] X. Hu, J. Wang, G. Wei, and X. Deng, "Decomposition of composite electric field in a three-phase D-dot voltage transducer measuring system," *Sensors*, vol. 16, no. 10, p. 1683, Oct. 2016.

- [67] D. Borkowski, A. Wetula, and A. Bien, "Contactless measurement of substation busbars voltages and waveforms reconstruction using electric field sensors and artificial neural network," *IEEE Trans. Smart Grid*, vol. 6, no. 3, pp. 1560–1569, May 2015.
- [68] F. Li and P. J. Moore, "Non-contact determination of the phase sequence and voltage level of overhead conductors in air insulated substations," *Int. J. Emerg. Electr. Power Syst.*, vol. 5, no. 1, pp. 623–628, Mar. 2006.
- [69] P. Issouribehere, D. Esteban, F. Issouribehere, G. Barbera, and H. Mayer, "Perturbation measurements on HV overhead lines using electric field sensors," in *Proc. IEEE Power Energy Soc. Gen. Meeting*, Vancouver, BC, Canada, Jul. 2013, pp. 1–5.
- [70] D. Voglitsis, N. P. Papanikolaou, and A. C. Kyritsis, "Active cross-correlation anti-islanding scheme for PV module-integrated converters in the prospect of high penetration levels and weak grid conditions," *IEEE Trans. Power Electron.*, vol. 34, no. 3, pp. 2258–2274, Mar. 2019.
- [71] *Electromagnetic Compatibility (EMC)—Part 4-7: Testing and Measurement Techniques—General Guide on Harmonics and Interharmonics Measurements and Instrumentation, for Power Supply Systems and Equipment Connected Thereto*, Standard 61000-4-7, Aug. 2002.
- [72] T. Lobos and J. Rezmer, "Real-time determination of power system frequency," *IEEE Trans. Instrum. Meas.*, vol. 46, no. 4, pp. 877–881, Aug. 1997.
- [73] O. Vainio and S. J. Ovaska, "Digital filtering for robust 50/60 hz zero-crossing detectors," *IEEE Trans. Instrum. Meas.*, vol. 45, no. 2, pp. 426–430, Apr. 1996.
- [74] *Electromagnetic Compatibility (EMC)—Part 4-30: Testing and Measurement Techniques—Power Quality Measurement Methods*, Standard 61000-4-30, Feb. 2015.
- [75] *IEEE Standard for Synchrophasor Measurements for Power Systems*, Standard C37.118.1-2011, Dec. 2011.



**Kun-Long Chen** (Member, IEEE) was born in New Taipei, Taiwan, in 1982. He received the B.S.E.E. degree from Feng-Chia University, Taichung, Taiwan, in 2004, and the M.S.E.E. and Ph.D. degrees from the National Taiwan University of Science and Technology (NTUST), Taipei, Taiwan, in 2006 and 2011, respectively.

From 2011 to 2015 and from 2019 to 2020, he was a Researcher with the Center for Measurement Standards (CMS), Industrial Technology Research Institute (ITRI), Hsinchu, Taiwan. From 2015 to 2016, he was a Post-Doctoral Fellow with the University of Alberta, Edmonton, AB, Canada. From 2016 to 2017, he was a Post-Doctoral Fellow with Energy Systems Research Center, University of Texas at Arlington, Arlington, TX, USA. From 2017 to 2019, he was a Qishan Scholar with the College of Electrical Engineering and Automation, Fuzhou University, Fuzhou, China. He is currently an Assistant Professor with the Department of Electrical Engineering, National Taiwan Ocean University, Keelung, Taiwan. His research interests include electronic instrument transformer, voltage and current sensors, high-voltage measurement technology, power metrology for smart grid, and nonintrusive load monitoring systems.



**Yi Guo** (Student Member, IEEE) received the B.S. degree in electrical engineering from Xi'an Jiaotong University, Xi'an, China, in 2013 and the M.S. degree in electrical engineering from the University of Michigan, Dearborn, MI, USA. He is currently pursuing the Ph.D. degree in mechanical engineering with The University of Texas at Dallas, Richardson, TX, USA.

His research interests are in control and optimization in networks, with applications to electric power networks.

**Juncheng Wang** (Graduate Student Member, IEEE) received the B.S.E.E. degree from Shanghai Jiao Tong University, Shanghai, China, in 2014 and the master's degree with the Department of Electrical and Computer Engineering, University of Alberta, Edmonton, AB, Canada, in 2017. He is currently pursuing the Ph.D. degree with the Department of Electrical and Computer Engineering, University of Toronto, Toronto, ON, Canada.

His research interest includes smart grid, adaptive sensor array technique, and power systems measurements.



**Xiangguo Yang** (Member, IEEE) was born in Hubei, Jianli, China, in 1981. He received the B.S.E.E., M.S.E.E., and Ph.D. degrees from Wuhan University (WHU), Wuhan, China, in 2004, 2006, and 2013, respectively.

From 2015 to 2017, he was a Post-Doctoral Fellow with the University of Alberta, Edmonton, AB, Canada. He is currently an Associate Professor with the School of Energy and Power Engineering, Wuhan University of Technology, Wuhan. His research interest is in power quality monitor analytics, control theory of power electronics, and microprocessor applications and smart grid.